

# In-situ Lithiated $\text{SiO}_2$ as Lithium-Free Anode for Lithium-Sulfur Batteries

Dasari Bosubabu,<sup>[a, b]</sup> Sampathkumar Ramakumar,<sup>[a]</sup> Sivaraj Jeevanantham,<sup>[a]</sup> Inthumathi Kanagaraj,<sup>[a]</sup> Pamula Balaji Bhargav,<sup>[c]</sup> Nafis Ahmed,<sup>[c]</sup> and Kannadka Ramesha<sup>\*[a, b]</sup>

Lithium-sulfur (Li–S) batteries are attractive owing to their high energy density and cost-effectiveness. However, the practical application of Li–S batteries is hindered by uncontrollable lithium dendrite growth and severe polysulfide shuttling during cycling. Here, we fabricated 100 nm thin  $\text{SiO}_2$  decorated on carbon cloth ( $\text{SiO}_2@\text{CC}$ ). It is observed that in-situ lithiation of  $\text{SiO}_2$  forms a highly lithiophilic  $\text{Li}_x\text{SiO}_y$  layer over  $\text{SiO}_2$  which further acts as an efficient host for dendrite-free lithium metal deposition. So lithiated  $\text{SiO}_2@\text{CC}$  shows high affinity for homogenous growth of Li while the carbon fibers control the volume change during the deposition/stripping process. Hence,

the synergistic effect of  $\text{Li}_x\text{SiO}_y$  layer and carbon cloth (CC) effectively suppresses dendritic Li growth. As a result, the symmetric cell exhibits an ultra-stable cycling performance over 1000 h with a low overpotential of  $<25$  mV even at a high current density of  $1 \text{ mA cm}^{-2}$ . Further, the lithiated  $\text{SiO}_2@\text{CC}$  is used as a lithium metal-free anode (also a flexible electrode) for Li–S battery, which exhibits a stable capacity of  $800 \text{ mAh g}^{-1}$  over 500 cycles due to its unique structural properties. This work offers new insights and paves the way for developing dendrite-free, high-performance Li–S battery technology.

## Introduction

There is significant demand for developing high energy density batteries for portable electronics, electric vehicles, and grid storage. Nevertheless, lithium-ion batteries (LIBs) have attained their maximum theoretical energy density limits hence further progress is sluggish for the last few years.<sup>[1,2]</sup> As a result, the development of alternative energy storage technologies (which are also termed as ‘beyond LIBs’) such as lithium metal batteries, lithium-sulfur batteries, and lithium-air batteries is necessary to accomplish the demand of modern society. More importantly, all of these high energy density systems utilize lithium metal as anode material, owing to its low gravimetric density ( $0.534 \text{ g cm}^{-3}$ ), lowest reduction potential ( $-3.04 \text{ V vs. SHE}$ ), and high specific capacity ( $3860 \text{ mAh g}^{-1}$ ,  $2061 \text{ mAh cm}^{-3}$ ) which is 10 times higher than traditional graphite anode material.<sup>[3]</sup> However, the practical application of lithium (Li) metal is severely impeded by the notorious Li dendrite formation, volume fluctuations, and rapid pulverization during electrochemical cycling processes.<sup>[4]</sup> Comprehensively, during the initial Li stripping/plating process, Li always forms a non-

uniform electrode/electrolyte interface with electrolyte due to the high activation energy of the Li metal ( $-8.670 \text{ kJ mol}^{-1}$  at room temperature).<sup>[4,5]</sup> This heterogeneous interface at the surface of Li possibly results in the inhomogeneous Li-ion diffusion, which is the origin of Li-nucleation (initiation of dendrite growth). In the subsequent cycles, a parasitic dendrite growth results in infinite volume change of the electrode. The dendrite formation and breaking results in loss of contact from the current collector. This dead Li is responsible for high resistance and high polarization of the cell. The above-mentioned problems eventually lead to an increased irreversible capacity loss, poor coulombic efficiency, and short lifespan.<sup>[6]</sup> Moreover, the direct growth of hazardous dendrite towards the cathode through separator causes the potential short circuit which brings safety limitations in the cells.<sup>[7]</sup>

Numerous research efforts have been dedicated in solving the above-mentioned issues viz., (i) establishing a stable SEI layer on the surface of Li by employing in-situ electrolyte additives.<sup>[8]</sup> For example, additives like lithium nitrate ( $\text{LiNO}_3$ ), lithium halide ( $\text{LiX}$ ), fluoroethylene carbonate (FEC), form a stable SEI layer that helps in uniform Li growth.<sup>[9–12]</sup> (ii) Introducing a physical artificial layer coating on Li metal surface. For example, the ex-situ surface coatings such as  $\text{LiF}$ ,  $\text{Li}_3\text{N}$ ,  $\text{LiPON}$ , polymer coatings, carbon materials, and lithiophilic material coatings have gained much interest.<sup>[8,13–19]</sup> In particular, lithiophilic material coating such as  $\text{ZnO}$ ,  $\text{CuO}$ ,  $\text{Si}$ ,  $\text{Ag}$ , and  $\text{Au}$  have superior advantages.<sup>[17,20–23]</sup> The higher lithiophilicity of these materials renders Li nucleation barrier, resulting in homogeneous Li deposition. Even though the above-mentioned strategies effectively control Li dendrite growth by forming the SEI layer, volume expansion (due to the internal stress fluctuations) and inhomogeneous Li deposition (due to the high local current densities) cannot be efficiently resolved by these simple surface

[a] Dr. D. Bosubabu, Dr. S. Ramakumar, S. Jeevanantham, I. Kanagaraj, Prof. K. Ramesha  
CSIR-Central Electrochemical Research Institute-Chennai Unit, CSIR-Madras Complex, Taramani, Chennai 600113, India  
E-mail: ramesha.cecrl@gmail.com

[b] Dr. D. Bosubabu, Prof. K. Ramesha  
Academy of Scientific and Innovative Research (AcSIR), CSIR-CECRI, Ghaziabad 201002, India

[c] Dr. P. B. Bhargav, Dr. N. Ahmed  
SSN Research Center, Sri Sivasubramaniya Nadar College of Engineering, Kalavakkam, 603110, India

 Supporting information for this article is available on the WWW under <https://doi.org/10.1002/batt.202200262>

modifications. Therefore, research has been directed to new strategies like (iii) adopting 3D porous materials that include 3D hollow carbon fiber,<sup>[24]</sup> 3D Cu,<sup>[25–27]</sup> 3D nickel foam<sup>[28,29]</sup> and graphene skeletons.<sup>[30–34]</sup> The high mechanical flexibility and huge conductive surface area of these materials offer low interfacial resistance; stable Li distribution, and low Li nucleation that leads to high Coulombic efficiency and cycling stability for Li-anodes.<sup>[8]</sup> Recently, Cheng et al. used a 3D glass fiber (GF) interlayer on the Cu foil. The SiO<sub>2</sub> present in the GF modified Cu foil controls the Li dendrite growth due to the strong interaction of Li with polar functional groups present in GF.

Here, we have utilized all three strategies together to overcome the problems arising when Li metal is used as an anode. In this work, we have coated ~100 nm thin lithiophilic SiO<sub>2</sub> on a 3D-carbon cloth (denoted as SiO<sub>2</sub>@CC) using Plasma Enhanced Chemical Vapour Deposition (PECVD). Further, a Li||Li symmetric cell is configured using SiO<sub>2</sub>@CC as an interlayer between the separator and one of Li electrodes. Interestingly, due to the excellent lithiophilicity of SiO<sub>2</sub>@CC, uniform Li distribution is observed during the Li stripping/deposition process. This results in high dendrite control over 1000 h at 1 mAh cm<sup>-2</sup> in the symmetric cell. Further, the in-situ lithiated SiO<sub>2</sub>@CC (obtained from cycled symmetric cell process) is used as an anode for Li–S battery applications. This Li metal-free Li–S battery shows stable initial discharge capacity of 900 mAh g<sup>-1</sup> and maintains its capacity to 770 mAh g<sup>-1</sup> over

500 cycles with an average capacity fade rate of only 0.04 % per cycle and coulombic efficiency of > 99%.

## Results and Discussion

### Morphology and structure

FESEM is employed to characterize the SiO<sub>2</sub> coated carbon cloth (SiO<sub>2</sub>@CC). Figure 1(a) shows the optical image including bare carbon cloth (black) and SiO<sub>2</sub> coated carbon cloth (dark gray) where the color change after SiO<sub>2</sub> coating is visible, since the SiO<sub>2</sub> source is SiH<sub>4</sub> gas in PECVD the coating is presumed as a uniform 3D coating (Figure S1). The SEM image of SiO<sub>2</sub>@CC is shown in Figure 1(b) where the CC consists of interwoven carbon fibers of 7–8 μm radius. The elemental mapping of SiO<sub>2</sub>@CC in Figure 1(c–e) revealed the homogeneous distribution of the Si and O in the SiO<sub>2</sub>@CC matrix. Further, Figure S2 shows high magnification FESEM and corresponding elemental mapping of CC. Figures S3 and S4 display FESEM and TEM images of SiO<sub>2</sub>@CC along with its elemental mapping, TEM image confirms the 45 nm thin SiO<sub>2</sub> coating over CC. The energy-dispersive X-ray diffraction (EDX) is used for elemental analysis of SiO<sub>2</sub>@CC, Figure 1(f) displays the signals from Si, O, and C of the spectra, and no other impurities are detected, further confirming thin SiO<sub>2</sub> is coated on carbon fibers of CC.

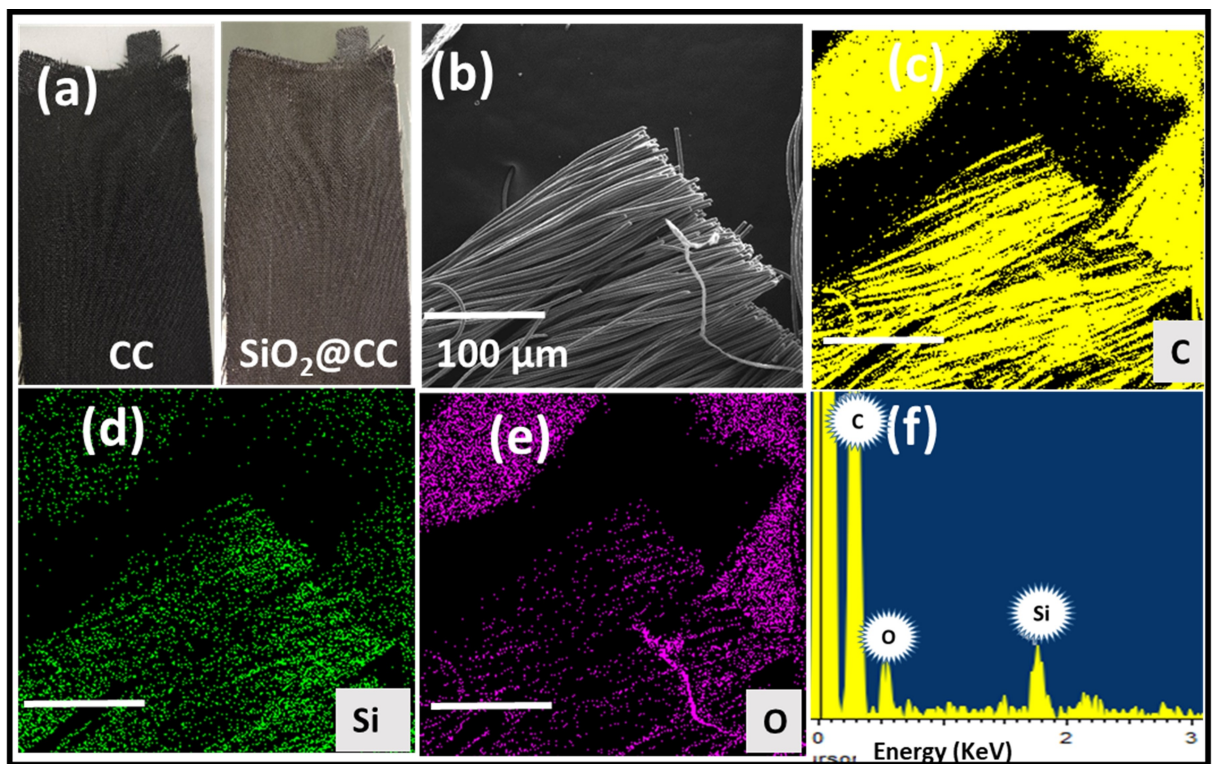


**Figure 1.** a) Optical image of carbon cloth (black) and SiO<sub>2</sub> coated carbon cloth (dark gray), b) FE-SEM images of SiO<sub>2</sub>@CC, and c–f) elemental mapping and EDX analysis of SiO<sub>2</sub>@CC

### Electrochemical performance of the symmetric cell

The swagelok cells with the configuration of  $\text{Li} \parallel \text{electrolyte} \parallel \text{SiO}_2@\text{CC-Li}$  and  $\text{Li} \parallel \text{electrolyte} \parallel \text{Li}$  were fabricated, celgard 2400 is used as a separator between the two electrodes. All the electrochemical characterizations are performed at room temperature and the electrolyte used is 1 M LiTFSI in DME/DOL and 0.25 M LiNO<sub>3</sub> is used as electrolyte additive. To avoid complexity, the potential advantages of LiNO<sub>3</sub> for dendrite stability are not discussed because it is used as an electrolyte additive in all the cells. EIS measurements were performed for as-fabricated fresh  $\text{Li} \parallel \text{Electrolyte} \parallel \text{Li}$  and  $\text{Li} \parallel \text{Electrolyte} \parallel \text{SiO}_2@\text{CC-Li}$  symmetric cells to ratify the influence of SiO<sub>2</sub>@CC-Li in enhancing the interface contact (Figure S5). The semicircle in the high-

frequency region specifies the interfacial resistance and the charge transfer resistance at the electrolyte/electrode interface. The  $\text{Li} \parallel \text{Electrolyte} \parallel \text{Li}$  symmetric cell showed an interface resistance of  $75 \Omega$ . On the contrary, the  $\text{Li} \parallel \text{Electrolyte} \parallel \text{SiO}_2@\text{CC-Li}$  symmetric cell displayed low interfacial resistance of  $30 \Omega$  due to the improved interface contact. Figure 2(a) shows lithium plating/stripping behavior of two symmetric cells ( $\text{Li} \parallel \text{electrolyte} \parallel \text{SiO}_2@\text{CC-Li}$ , and  $\text{Li} \parallel \text{electrolyte} \parallel \text{Li}$  cells) at a current density of  $1 \text{ mA cm}^{-2}$  for a time duration of 1000 h. Though both the cells show similar overpotential (30 mV) within the potential window ( $-0.2$  and  $+0.2$  V) but the plating/stripping plateaus are different (Figure 2b) which indicates that the lithium plating/stripping mechanism is different in these two cells. After 250 h, the  $\text{Li} \parallel \text{electrolyte} \parallel \text{Li}$  cell displays larger

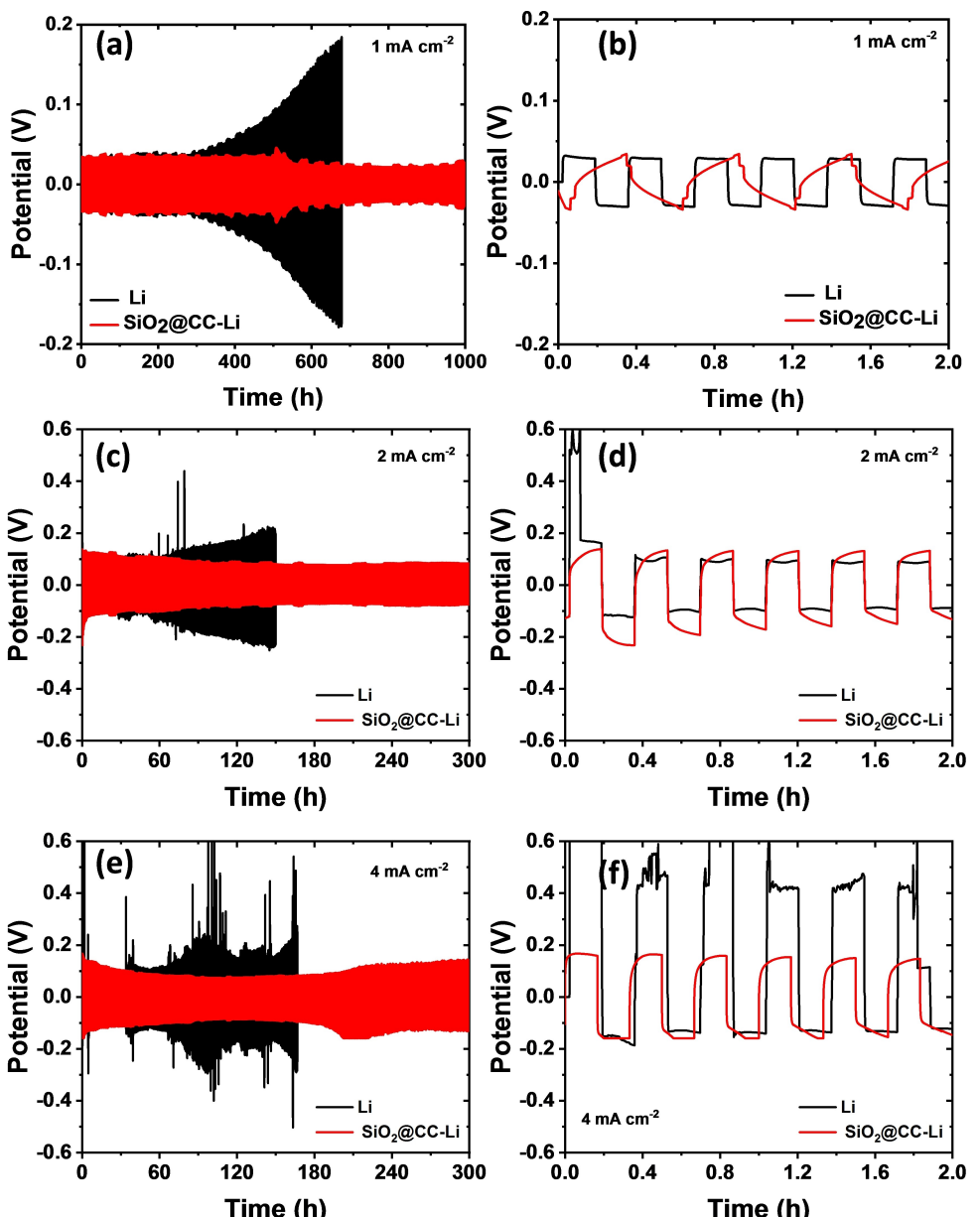


**Figure 2.** Comparison of lithium stripping/plating voltage profile of  $\text{Li} \parallel \text{electrolyte} \parallel \text{Li}$  and  $\text{Li} \parallel \text{electrolyte} \parallel \text{SiO}_2@\text{CC-Li}$  cells at various constant current densities: a and b)  $1 \text{ mA cm}^{-2}$ , c and d)  $2 \text{ mA cm}^{-2}$  and e and f)  $4 \text{ mA cm}^{-2}$  measured at room temperature.

polarization (about 50–180 mV) that increases with time, this can be attributed to the continuous stripping/ plating process creating volume expansion followed by the non-uniform SEI layer which results in heterogeneous Li deposition. Whereas, the  $\text{Li} \parallel \text{electrolyte} \parallel \text{SiO}_2@\text{CC}-\text{Li}$  symmetric cell even after 1000 h cycling displayed a relatively stable  $\text{Li}^+$  stripping/plating along with a stable polarization voltage range of 25 mV as shown in Figure 2(a), which represents a homogeneous current distribution at the interface. Further, the cells are also tested at higher currents of 2 and 4  $\text{mA cm}^{-2}$ , and their comparison is shown in Figures 2 and S6. As shown in Figure 2(c–f), the  $\text{Li} \parallel \text{Electrolyte} \parallel \text{Li}$  cell displays an uneven voltage response at higher current, which indicates the non-uniform stripping/plating process even from the initial runs. In general, a higher current density is more prone to develop short circuits because the path of conductive Li growth is much higher towards the separator. Whereas, the  $\text{Li} \parallel \text{electrolyte} \parallel \text{SiO}_2@\text{CC}-\text{Li}$  symmetric cell displayed outstanding cycling stability even at higher current densities of 2 and 4  $\text{mA cm}^{-2}$ . This is due to the low conductivity of  $\text{SiO}_2$  resulting in sluggish lithium growth by minimizing the local current density on the Li, and also the inherent space in carbon cloth can control the volume changes during Li deposition. Therefore, the excellent homogeneous stable plating/stripping observed for the  $\text{Li} \parallel \text{Electrolyte} \parallel \text{SiO}_2@\text{CC}-\text{Li}$  symmetric cell could be credited to the uniform contact established by the  $\text{SiO}_2@\text{CC}$ . The observed polarization

voltages of  $\text{Li} \parallel \text{Electrolyte} \parallel \text{SiO}_2@\text{CC}-\text{Li}$  cell after the 300<sup>th</sup> cycle were 0.09 V and 0.11 V, at current densities of 2 and 4  $\text{mA cm}^{-2}$ , respectively. This lends support to the observation that the  $\text{SiO}_2@\text{CC}$  interlayer efficiently stabilizes the interface signifying uniform lithium-ion flow across the interface. The above results evoke the controlled volume change as a result of the synergistic effect arising from the presence of 3D architecture CC and lithiophilic  $\text{SiO}_2$  which enable an ultra-stable cycling performance even at a higher current density.

### Postmortem analysis of the symmetric cell

Considering the high electrochemical stability of the  $\text{Li} \parallel \text{electrolyte} \parallel \text{SiO}_2@\text{CC}-\text{Li}$  symmetric cell, the chemical changes that occur in  $\text{SiO}_2@\text{CC}$  during the lithiation are investigated using ex-situ XPS analysis. The XPS analyses are carried out on pristine and cycled samples (of 12 h and 250 h). The cells are opened inside the glovebox; the electrodes are thoroughly washed with electrolyte solvent and dried in the glovebox. The high-resolution XPS spectra of the pristine  $\text{SiO}_2@\text{CC}$  and after 12 h cycled, and after 250 h cycled lithiated  $\text{SiO}_2@\text{CC}$  samples are shown in Figure 3(a and b). For the pristine sample, the Si2p displayed a peak at 104.1 eV, which represents the +4 oxidation state of Si in  $\text{SiO}_2$ . After lithiation (i.e., for 12 h), the peak shifted to lower binding energy (100.6 eV) suggesting the

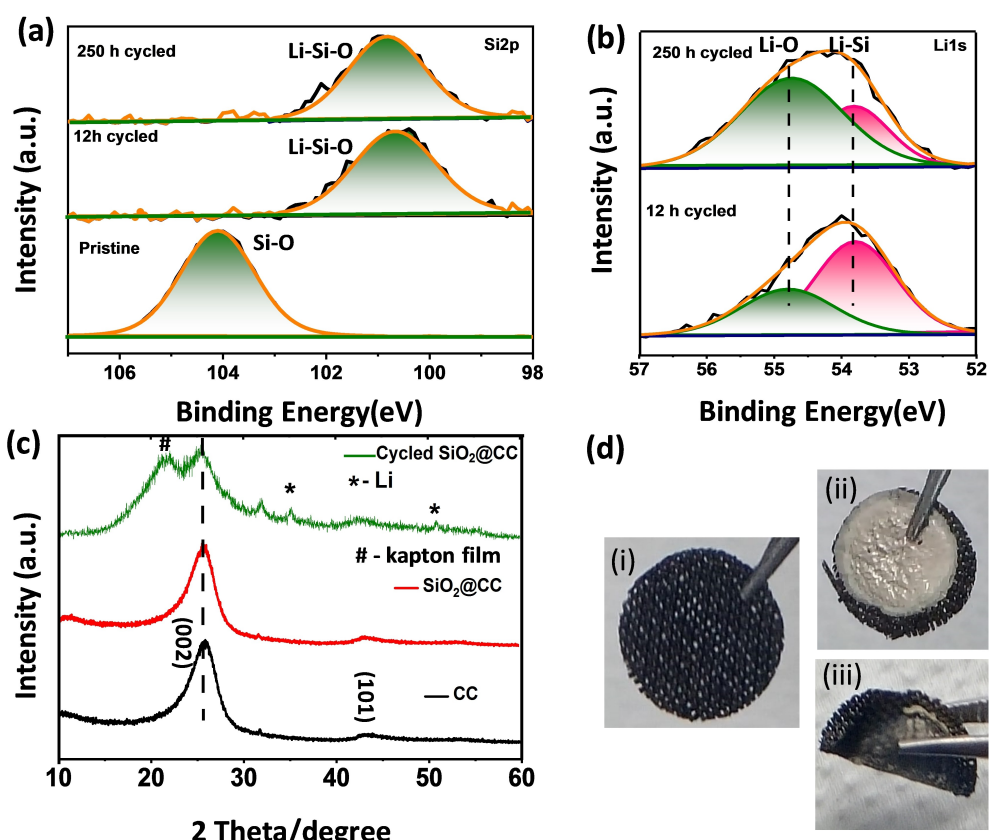


**Figure 3.** a) XPS spectra of Si 2P: pristine, after 12 h and 250 h of cycled  $\text{SiO}_2@\text{CC}$ , b) XPS spectra of Li1s: after 12 h and 250 h of cycled  $\text{SiO}_2@\text{CC}$ , c) XRD pattern of bare CC, pristine  $\text{SiO}_2@\text{CC}$ , and cycled  $\text{SiO}_2@\text{CC}$ , and d) photographs of (i) fresh  $\text{SiO}_2@\text{CC}$ , (ii) cycled  $\text{SiO}_2@\text{CC}$  after 300 cycles, (iii) flexibility of the cycled  $\text{SiO}_2@\text{CC}$ .

reduction of  $\text{SiO}_2$  to  $\text{Li}_x\text{SiO}_y$  by forming a Si–Li bond. The  $\text{Li}_x\text{SiO}_y$  is one of the products that occurred in the irreversible conversion reaction of  $\text{SiO}_x$  in the first cycle. The 250 h cycling data reveals that this peak remains stable which further confirms, that lithiation is effective and stable. The XPS analysis of Li is carried out for the “12 h cycled” and “after 250 h cycled” samples. The peak at 54.7 eV is attributed to the presence of  $\text{Li}_2\text{O}$  and the peak at 53.8 eV is due to the Li–Si bond.<sup>[35]</sup> The XPS analysis concludes the formation of irreversible  $\text{Li}_x\text{SiO}_y$  over the CC.<sup>[36–40]</sup>

The XRD pattern of bare CC,  $\text{SiO}_2@\text{CC}$ , and 250 h cycled  $\text{SiO}_2@\text{CC}$  is shown in Figure 3(c). As shown in the XRD pattern, the characteristic peaks at  $26^\circ$  and  $43^\circ$  can be ascribed to (002) and (101) planes of CC. Unfortunately, the  $\text{SiO}_2$  peaks are unidentified due to the overlapping reflection regions with CC.

In addition to CC peaks, the cycled  $\text{SiO}_2@\text{CC}$  sample displays two extra peaks at  $36.2^\circ$  and  $52.2^\circ$  which matches the reflections of  $\text{Li}_4\text{SiO}_4$ . This confirms that the coated  $\text{SiO}_2$  is lithiated to  $\text{Li}_4\text{SiO}_4$  on the surface of CC. Figure 3(d) shows the photographic images of the fresh  $\text{SiO}_2@\text{CC}$  and the cycled  $\text{SiO}_2@\text{CC}$  over 300 cycles, the lithophilic nature of  $\text{SiO}_2@\text{CC}$  can be visible by forming a thick layer of lithium during cycling which can be easily curved with tweezers. The electrodes showed very good flexibility, which makes them a suitable candidate for application in flexible devices.

Further, the postmortem SEM analysis of cycled  $\text{Li}||\text{electrolyte}||\text{Li}$ , and  $\text{Li}||\text{electrolyte}||\text{SiO}_2@\text{CC}-\text{Li}$  cells was carried out (Figure 4). The disassembled, cycled lithium and lithiated  $\text{SiO}_2@\text{CC}-\text{Li}$  was protected from atmospheric air before the SEM analysis. The photographic images in Figure 4 (a and b)

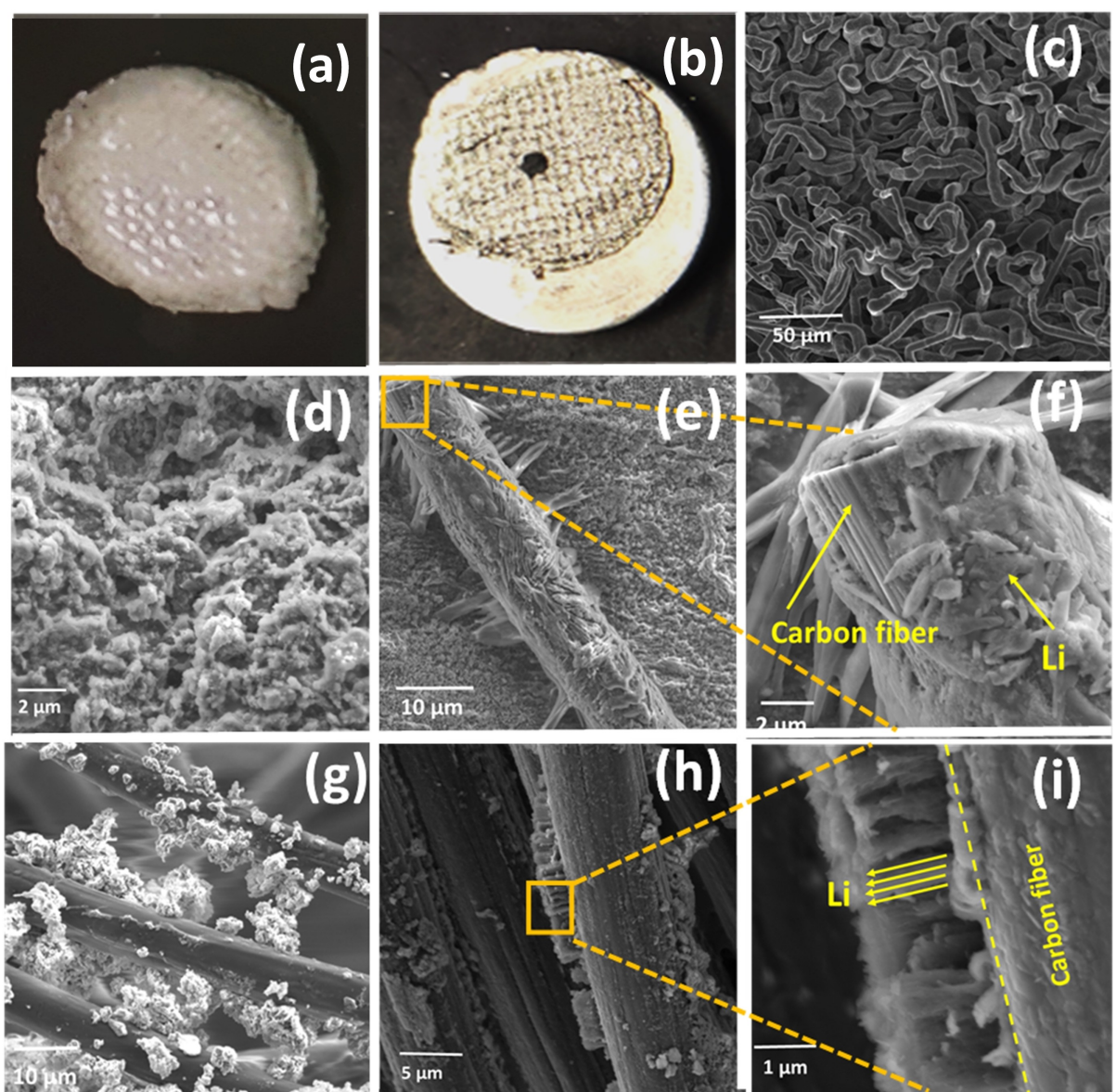


**Figure 4.** a, c) photograph and FE-SEM images of Li metal in  $\text{Li}||\text{electrolyte}||\text{Li}$  after 250 h cycling. b, d) photograph and FE-SEM images of Li metal in  $\text{Li}||\text{electrolyte}||\text{SiO}_2@\text{CC}-\text{Li}$  symmetric cells after 250 h cycling. e, f) enlarged SEM of center area of (b). g) Trapped lithium inside the  $\text{SiO}_2@\text{CC}$ . h, i) lithium growth on the surface of cycled  $\text{SiO}_2@\text{CC}$ .

represents the 250 h cycled both unprotected Li from the Li||electrolyte||Li cell and the protected Li from Li||electrolyte||SiO<sub>2</sub>@CC-Li cell. The changes in both the cells are evident. The Li from non-protected cell Li||electrolyte||Li (Figure 4a) shows deposition of irregular lithium that exists on the surface of the Li matrix owing to the inhomogeneous deposition of lithium (lithium dendrite). Whereas the SiO<sub>2</sub>@CC protected cycled lithium (Figures 4b, S7), the surface resembles fresh lithium even after 250 h cycling. The corresponding SEM images are shown in Figure 4(c, d). Figures 4(c) and S4(d-f) show the lithium dendrite on the surface of lithium (towards the separator side) in the Li||electrolyte||Li cell, which might be responsible for higher overpotential of the cell. Besides, the SiO<sub>2</sub>@CC protected cycled lithium in Li||electrolyte||SiO<sub>2</sub>@CC-Li cell is clear and resembles fresh lithium (Figure 4d). This is attributed to the lithiophilic sites present on polar SiO<sub>2</sub>@CC that attract lithium during the stripping/ plating process and keep lithium metal as a fresh electrode always.<sup>[41]</sup> Interestingly, in this cell, some of the SiO<sub>2</sub>@CC is stuck in the Li metal, the corresponding SEM of this black-spotted area in Figure 4(b) is enlarged and shown in Figure 4(e and f), which reveals that the carbon fiber is stuck on the surface of the lithium electrode. Figure 4(g) shows the cycled SiO<sub>2</sub>@CC. Remarkably, during the continuous cycling process, the porous structure of carbon cloth not only controls the volume buffering but also helps in storing most of the cycled lithium in the available free space. This will be more beneficial to use as a self-standing anode in the Li-S full cell battery (discussed below). The higher magnification SEM images of lithiated SiO<sub>2</sub>@CC are shown in Figure 4(h and i). Here, it is visible that Li

grew on the surface of SiO<sub>2</sub>@CC-Li, which demonstrates the lithiophilic nature of the fibers. The enlarged region shows that the grown lithium is more than 1 μm in thickness. The SiO<sub>2</sub> is highly lithiophilic in nature which helps in reducing the energy barrier needed to overcome the nucleation and deposition of lithium ions thereby controlling the dendrite growth in Li||electrolyte||SiO<sub>2</sub>@CC-Li cell. The SEM analysis concludes that lithiated SiO<sub>2</sub>@CC architecture maintains its overall morphology during cycling leading to an excellent electrochemical performance by holding a huge amount of cycled metallic lithium and helping the electrode from the dendrite.

The schematic illustration of Li||electrolyte||Li, and Li||electrolyte||SiO<sub>2</sub>@CC-Li cells are shown as Figure 5. The Li||electrolyte||Li cell shows lithium dendrite growth towards the separator during cycling, whereas in Li||electrolyte||SiO<sub>2</sub>@CC-Li cell lithiated SiO<sub>2</sub>@CC acts as a lithiophilic layer and controls lithium growth to one dimension and distributes to over 3 dimensions of carbon fibers, resulting in trapping cycled lithium inside the interlayer.

#### Electrochemical performance of full cell with lithiated SiO<sub>2</sub>@CC anode

The practical application of Li-battery requires optimal quantity of Li metal at anode based on the ratio of the anode to cathode capacity. Nevertheless, in lithium metal batteries excess quantity of lithium metal is used which not only increases the cost but also imparts unwanted parasitic reactions and also raises safety issues. The direct use of lithiated 3D design eliminates

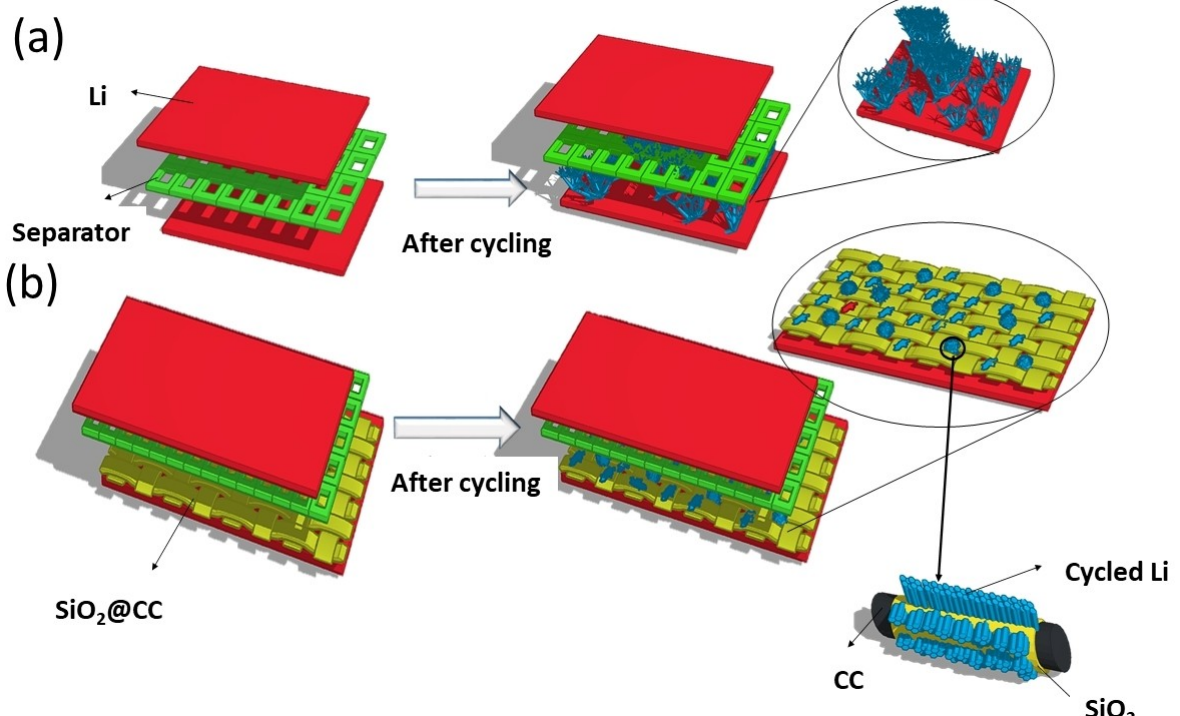
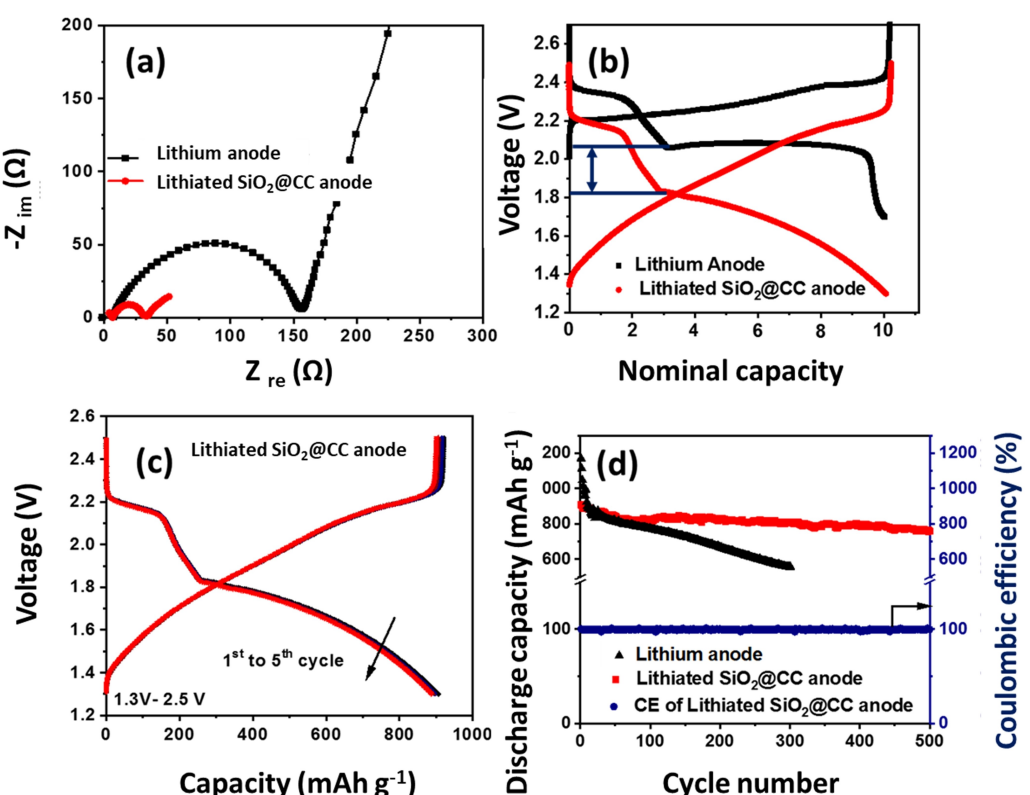


Figure 5. The schematic illustration of Li||electrolyte||Li, and Li||electrolyte||SiO<sub>2</sub>@CC-Li cells.

the practice of using a high amount of Li metal. Moreover, the porous 3D design makes it appropriate for higher energy density applications. As discussed before the lithiated  $\text{SiO}_2@\text{CC}$  electrode has high amount of deposited and surface-grown lithium which can be used as a self-standing anode for battery application. For this purpose, a symmetric cell ( $\text{Li}||\text{Electrolyte}||\text{SiO}_2@\text{CC}-\text{Li}$ ) after 250 h cycling, is opened and the flexible lithiated  $\text{SiO}_2@\text{CC}$  electrode is removed, and washed with electrolyte solvent multiple times, and used as fresh anode for Li-S battery construction. Moreover, this lithiated  $\text{SiO}_2@\text{CC}$  electrode eliminates the need of Cu current collector, binder, and an excess presence of lithium as foil, thus facilitating a robust cell configuration for high energy density and safe battery applications. Hence, the full cell is constructed with free-standing sulfur paper (synthesis process is given in Supporting Information) as a cathode with an areal sulfur loading of  $2 \text{ mg cm}^{-2}$ , and the lithiated  $\text{SiO}_2@\text{CC}$  as an anode, so the cell configuration can be written as lithiated  $\text{SiO}_2@\text{CC}||\text{electrolyte}||\text{S}$ . For comparison the traditional  $\text{Li}||\text{electrolyte}||\text{S}$  cell with lithium metal foil as anode is also tested. The electrochemical performance was measured at a current density of C/5, with 1 M LiTFSI dissolved in DME and DOL (1:1 V/V%) as electrolyte and 0.25 M  $\text{LiNO}_3$  as an additive. Importantly, in the case of  $\text{Li}||\text{electrolyte}||\text{S}$  cell the voltage window is limited to 1.7–2.7 V vs.  $\text{Li}/\text{Li}^+$  whereas the voltage window of lithiated  $\text{SiO}_2@\text{CC}||\text{electrolyte}||\text{S}$  cell is limited to 1.3–2.5 V vs.  $\text{Li}/\text{Li}^+$ . This is because the lithiated  $\text{SiO}_2@\text{CC}$  anode

shows 0.2 V lesser potential than that for Li anode which further confirms that the constructed cell is different from the traditional Li-S battery.

The electrochemical impedance spectroscopy (EIS) measurements were carried out for lithiated  $\text{SiO}_2@\text{CC}||\text{electrolyte}||\text{S}$  and  $\text{Li}||\text{electrolyte}||\text{S}$  cells, and are shown in Figure 6(a). Both the impedance spectra displayed a large semicircle in the high-frequency range followed by an inclined line in the low-frequency region indicating the solid-state diffusion. The interfacial charge-transfer resistance ( $R_{ct}$ ) for the cell lithiated  $\text{SiO}_2@\text{CC}||\text{electrolyte}||\text{S}$  is much lower ( $32 \Omega$ ) than that of pristine lithium anode suggesting reduced polarization and improved charge transport by the introduction of lithiated  $\text{SiO}_2@\text{CC}$ . Figure 6(b) shows the voltage vs. nominal capacity plot of lithiated  $\text{SiO}_2@\text{CC}||\text{electrolyte}||\text{S}$  and  $\text{Li}||\text{electrolyte}||\text{S}$  cells. Both cells show similar two plateaus as commonly observed for the Li-S system, the higher voltage plateau represents the conversion of higher-order polysulfides to lower-order polysulfides ( $\text{Li}_2\text{S}_n$ ,  $4 < n \leq 8$ ) and the lower voltage plateau represents lower-order polysulfides to  $\text{Li}_2\text{S}_2/\text{Li}_2\text{S}$  ( $\text{Li}_2\text{S}_n$ ,  $1 < n \leq 4$ ).<sup>[42–49]</sup> However, in the case of lithiated  $\text{SiO}_2@\text{CC}||\text{electrolyte}||\text{S}$  full cell, the charge-discharge cycling curves are pushed downwards by 0.2 V in the potential axis compared to Li-metal anode cell. This change indicates that the cycling behavior of lithiated  $\text{SiO}_2@\text{CC}||\text{electrolyte}||\text{S}$  full cell is different from the  $\text{Li}||\text{electrolyte}||\text{S}$  cell. This confirms that  $\text{Li}_x\text{SiO}_y$  on CC acts as anode and not the trapped Li in CC matrix.



**Figure 6.** a) Nyquist plot of  $\text{Li}||\text{electrolyte}||\text{S}$  and lithiated  $\text{SiO}_2@\text{CC}||\text{electrolyte}||\text{S}$  cells, b) comparison of charge-discharge curves of  $\text{Li}||\text{electrolyte}||\text{S}$  and lithiated  $\text{SiO}_2@\text{CC}||\text{electrolyte}||\text{S}$  cells, c) stable charge-discharge profile of lithiated  $\text{SiO}_2@\text{CC}||\text{electrolyte}||\text{S}$  cell and d) capacity vs. cycle number for  $\text{Li}||\text{electrolyte}||\text{S}$  and lithiated  $\text{SiO}_2@\text{CC}||\text{electrolyte}||\text{S}$  cells. Coulombic efficiency of lithiated  $\text{SiO}_2@\text{CC}||\text{electrolyte}||\text{S}$  cell was also shown.

The initial five charge-discharge cycles of lithiated  $\text{SiO}_2@\text{CC}||\text{electrolyte}||\text{S}$  full cell is shown in Figure 6(c) which convey a stable cycling behavior. The long term cycling stability vs. cycle number of lithiated  $\text{SiO}_2@\text{CC}||\text{electrolyte}||\text{S}$  and  $\text{Li}||\text{electrolyte}||\text{S}$  cells are compared in Figure 6(d). The lithiated  $\text{SiO}_2@\text{CC}$  cell shows a nearly similar discharge capacity to that of  $\text{Li}||\text{electrolyte}||\text{S}$  during the initial cycles. However, it exhibits much better capacity retention. The lithiated  $\text{SiO}_2@\text{CC}$  anode cell delivers a higher initial discharge capacity of  $900 \text{ mAh g}^{-1}$  and maintains its capacity to  $770 \text{ mAh g}^{-1}$  over 500 cycles with an average capacity fade rate of only  $0.04\%$  per cycle. The enhanced cyclability of lithiated  $\text{SiO}_2@\text{CC}||\text{electrolyte}||\text{S}$  can be attributed to the unique structure, strong interfacial adhesion strength, and robust mechanical properties of the lithiated  $\text{SiO}_2@\text{CC}$  anode.<sup>[40,50]</sup> On the other hand, the  $\text{Li}||\text{electrolyte}||\text{S}$  cell experiences deprived cycling performance with rapid capacity decay, retaining a capacity of only  $400 \text{ mAh g}^{-1}$  after 300 cycles. This indicates that cell degradation not only depends on the polysulfide shuttle but also depends on the anode stability. Moreover, the lithiated  $\text{SiO}_2@\text{CC}-\text{Li}||\text{electrolyte}||\text{S}$  cell demonstrate stable coulombic efficiency of  $>99\%$  over 500 cycles. This stable behavior reveals that  $\text{SiO}_2@\text{CC}$  can act as an efficient lithium storage host by mitigating parasitic reactions of the lithium metal.

## Conclusion

The effect of  $\text{SiO}_2$  layer coated on carbon cloth as an efficient interlayer for lithium batteries has been studied. The cell with  $\text{SiO}_2@\text{CC}$  interlayer outperform Li metal anode for over 1000 cycles at a current density of  $1 \text{ mA cm}^{-2}$ . Further, the cell displayed high stability even at a higher current density of 2 and  $4 \text{ mA cm}^{-2}$ . The XRD and XPS confirm that the  $\text{SiO}_2$  present on carbon cloth converted to  $\text{Li}_4\text{SiO}_4$  during cycling. This in-situ formed interlayer acts as a lithiophilic site and lithiated  $\text{SiO}_2@\text{CC}$  acts as a promising host structure for lithium deposition. This robust interlayer is not only capable of controlling the volume change during stripping/plating process but also suppresses the lithium dendrite growth. So lithiated  $\text{SiO}_2@\text{CC}$  can be used as an anode for the Li–S battery which shows stable cycling behavior over 500 cycles, with a discharge capacity of  $770 \text{ mAh g}^{-1}$ . This work offers new insights and paves the way for developing dendrite-free, high-performance Li–S battery technology.

## Supporting Information

Experimental section, FESEM and elemental mapping of CC, FESEM, TEM and elemental mapping of  $\text{SiO}_2@\text{CC}$ , Impedance measurement of pristine and  $\text{SiO}_2@\text{CC}$  interlayer, Comparison of stripping/plating profile of  $\text{SiO}_2@\text{CC}$  interlayer at different currents, FE-SEM images of fresh and cycled Li and  $\text{SiO}_2@\text{CC}$  interlayer containing Li, cathode synthesis procedure, structural characterization, electrochemical characterization details.

## Notes

CSIR-CECRI manuscript communication number: CECRI/PESVC/Pubs/2022-057.

## Acknowledgements

D.B.B. expresses his thanks to CSIR, New Delhi, India for the award of CSIR-UGC fellowship [No. 23/12/2012(ii) EU–V]. S.R. acknowledges SERB, New Delhi for the award of Young Scientist (File No. YSS/2015/000967). S.J. thanks CSIR, India for CSIR-SRF Fellowship (Grant No-31/20(0183)/2019- EMR-I). The authors thank the Central Instrumentation Facility, CECRI, Karaikudi, CSIR, India, for providing characterization facilities.

## Data Availability Statement

The data that support the findings of this study are available from the corresponding author upon reasonable request.

## Conflict of Interest

The authors declare no conflict of interest.

**Keywords:** lithium-sulfur (Li–S) battery • lithium symmetric cells • metal-free anode •  $\text{SiO}_2$  coating • sulfur cathode

- [1] X. Zhang, Y. Yang, Z. Zhou, *Chem. Soc. Rev.* **2020**, *49*, 3040.
- [2] X.-B. Cheng, J.-Q. Huang, Q. Zhang, *J. Electrochem. Soc.* **2018**, *165*, A6058.
- [3] X. B. Cheng, R. Zhang, C. Z. Zhao, Q. Zhang, *Chem. Rev.* **2017**, *117*, 10403.
- [4] Q. Yan, G. Whang, Z. Wei, S. T. Ko, P. Sautet, S. H. Tolbert, B. S. Dunn, J. Luo, *Appl. Phys. Lett.* **2020**, *117*, 194702.
- [5] E. Peled, *J. Electrochem. Soc.* **1979**, *126*, 2047.
- [6] D. Aurbach, E. Zinigrad, Y. Cohen, H. Teller, *Solid State Ionics* **2002**, *148*, 405.
- [7] S. Xia, X. Wu, Z. Zhang, Y. Cui, W. Liu, *Chem* **2019**, *5*, 753.
- [8] Y. Feng, C. Zhang, B. Li, S. Xiong, J. Song, *J. Mater. Chem. A* **2019**, *7*, 6090.
- [9] A. Rosenman, R. Elazari, G. Salitra, E. Markevich, D. Aurbach, A. Garsuch, *J. Electrochem. Soc.* **2015**, *162*, A470.
- [10] S. Xiong, M. Regula, D. Wang, J. Song, *Electrochem. Energy Rev.* **2018**, *1*, 388.
- [11] H. Zhang, G. G. Eshetu, X. Judez, C. Li, L. M. Rodriguez-Martínez, M. Armand, *Angew. Chem. Int. Ed.* **2018**, *57*, 15002.
- [12] S. Thieme, J. Brückner, A. Meier, I. Bauer, K. Gruber, J. Kaspar, A. Helmer, H. Althues, M. Schmuck, S. Kaskel, *J. Mater. Chem. A* **2015**, *3*, 3808.
- [13] K. Park, J. B. Goodenough, *Adv. Energy Mater.* **2017**, *7*, 1700732.
- [14] K. Il Chung, W. S. Kim, Y. K. Choi, *J. Electroanal. Chem.* **2004**, *566*, 263.
- [15] J. Lopez, A. Pei, J. Y. Oh, G. J. N. Wang, Y. Cui, Z. Bao, *J. Am. Chem. Soc.* **2018**, *140*, 11735.
- [16] X. Yang, Y. Peng, J. Hou, Y. Liu, X. Jian, *Nanotechnol. Rev.* **2020**, *9*, 1610.
- [17] Z. Zuo, L. Zhuang, J. Xu, Y. Shi, C. Su, P. Lian, B. Tian, *Front. Chem.* **2020**, *8*, 1.
- [18] M. C. Stan, J. Becking, A. Kolesnikov, B. Wankmiller, J. E. Frerichs, M. R. Hansen, P. Bieker, M. Kolek, M. Winter, *Mater. Today* **2020**, *39*, 137.
- [19] L. Tan, C. Wei, Y. Zhang, Y. An, S. Xiong, J. Feng, *Chem. Eng. J.* **2022**, *442*, 136243.

- [20] H. Zhang, X. Liao, Y. Guan, Y. Xiang, M. Li, W. Zhang, X. Zhu, H. Ming, L. Lu, J. Qiu, Y. Huang, G. Cao, Y. Yang, L. Mai, Y. Zhao, H. Zhang, *Nat. Commun.* **2018**, *9*, 1.
- [21] J. Cao, L. Deng, X. Wang, W. Li, Y. Xie, J. Zhang, S. Cheng, *Energy Fuels* **2020**, *34*, 7684.
- [22] Z. Liang, D. Lin, J. Zhao, Z. Lu, Y. Liu, C. Liu, Y. Lu, H. Wang, K. Yan, X. Tao, Y. Cui, *Proc. Natl. Acad. Sci. USA* **2016**, *113*, 2862.
- [23] M. C. Stan, J. Becking, A. Kolesnikov, B. Wankmiller, J. E. Frerichs, M. R. Hansen, P. Bieker, M. Kolek, M. Winter, *Mater. Today* **2020**, *39*, 137.
- [24] Y. Zhang, Y. Shi, X. C. Hu, W. P. Wang, R. Wen, S. Xin, Y. G. Guo, *Adv. Energy Mater.* **2020**, *10*, 1.
- [25] F. Shen, F. Zhang, Y. Zheng, Z. Fan, Z. Li, Z. Sun, Y. Xuan, B. Zhao, Z. Lin, X. Gui, X. Han, Y. Cheng, C. Niu, *Energy Storage Mater.* **2018**, *13*, 323.
- [26] Q. Li, S. Zhu, Y. Lu, *Adv. Funct. Mater.* **2017**, *27*, 1606422.
- [27] C. P. Yang, Y. X. Yin, S. F. Zhang, N. W. Li, Y. G. Guo, *Nat. Commun.* **2015**, *6*, 8058.
- [28] S. Sen Chi, Y. Liu, W. L. Song, L. Z. Fan, Q. Zhang, *Adv. Funct. Mater.* **2017**, *27*, 1.
- [29] Q. Zhang, W. L. Bai, C. Y. Sun, X. Liu, K. X. Wang, J. S. Chen, *Chem. Eng. J.* **2021**, *405*, 127022.
- [30] G. Huang, J. Han, F. Zhang, Z. Wang, H. Kashani, K. Watanabe, M. Chen, *Adv. Mater.* **2019**, *31*, 1.
- [31] R. Mukherjee, A. V. Thomas, D. Datta, E. Singh, J. Li, O. Eksik, V. B. Shenoy, N. Koratkar, *Nat. Commun.* **2014**, *5*.
- [32] F. Ni, Y. Ma, J. Chen, W. Luo, J. Yang, *Chin. Chem. Lett.* **2021**, *32*, 2073.
- [33] G. Zhu, R. Guo, W. Luo, H. K. Liu, W. Jiang, S. X. Dou, J. Yang, *Natl. Sci. Rev.* **2021**, *8*, 152.
- [34] F. Z. Zhang, Y. Y. Ma, M. M. Jiang, W. Luo, J. P. Yang, *Rare Met.* **2022**, *41*, 1276.
- [35] C. Shen, R. Fu, Y. Xia, Z. Liu, *RSC Adv.* **2018**, *8*, 14473.
- [36] H. J. Kim, S. Choi, S. J. Lee, M. W. Seo, J. G. Lee, E. Deniz, Y. J. Lee, E. K. Kim, J. W. Choi, *Nano Lett.* **2016**, *16*, 282.
- [37] B. Philippe, R. Dedryvère, J. Allouche, F. Lindgren, M. Gorgoi, H. Rensmo, D. Gonbeau, K. Edström, *Chem. Mater.* **2012**, *24*, 1107.
- [38] D. Bosu, R. N. Ramesha, P. Masthanaiah, A. Kaitheri, N. Kumar, A. Arulraj, K. Ramesha, *J. Power Sources* **2019**, *436*, 226870.
- [39] Z. Meng, Z. Li, L. Wang, T. Diemant, D. Bosababu, Y. Tang, R. Berthelot, Z. Zhao-Karger, M. Fichtner, *ACS Appl. Mater. Interfaces* **2021**, *13*, 37044.
- [40] P. Masthanaiah, D. B. Babu, M. L. Roy, K. Ramesha, *J. Power Sources* **2019**, *436*, 226850.
- [41] F. Guo, C. Wu, H. Chen, F. Zhong, X. Ai, H. Yang, J. Qian, *Energy Storage Mater.* **2020**, *24*, 635.
- [42] D. Bosababu, R. Sampathkumar, G. Karkera, K. Ramesha, *Energy Fuels* **2021**, *35*, 8286.
- [43] D. B. Babu, K. Ramesha, *Carbon* **2019**, *144*, 582.
- [44] D. Bosababu, J. Sivaraj, R. Sampathkumar, K. Ramesha, *ACS Appl. Energ. Mater.* **2019**, *2*, 4118.
- [45] D. B. Babu, K. Giribabu, K. Ramesha, *ACS Appl. Mater. Interfaces* **2018**, *10*, 19721.
- [46] D. Bosababu, J. Sivaraj, P. Gurunathan, K. Ramesha, *Energy Fuels* **2020**, *34*, 16810.
- [47] G. Angamuthu, D. Bosu, K. Ramesha, V. Rangarajan, *J. Electroanal. Chem.* **2019**, *843*, 37.
- [48] G. Angamuthu, D. Bosababu, K. Ramesha, V. Rengarajan, *Appl. Mater. Res.* **2021**, *22*, 100916.
- [49] J. Sivaraj, D. Bosababu, K. Ramesha, *Energy Fuels* **2022**, *36*, 2202.
- [50] D. Bosababu, Z. Li, Z. Meng, L. P. Wang, M. Fichtner, Z. Zhao-Karger, *J. Mater. Chem. A* **2021**, *9*, 25150.

Manuscript received: June 18, 2022

Revised manuscript received: August 11, 2022

Accepted manuscript online: August 12, 2022

Version of record online: September 7, 2022